OPEN ACCESS

University of BRISTOL

Wang, J., Hedayati, M., Liu, D., Adami, S-E., Dymond, H., Dalton, J., & Stark, B. (2018). Infinity Sensor: Temperature Sensing in GaN Power Devices using Peak di/dt. In *2018 IEEE Energy Conversion Congress and Exposition (ECCE 2018)* (pp. 884-890). Institute of Electrical and Electronics Engineers (IEEE). https://doi.org/10.1109/ECCE.2018.8558287

Peer reviewed version

Link to published version (if available):
10.1109/ECCE.2018.8558287

Link to publication record in Explore Bristol Research
PDF-document

University of Bristol - Explore Bristol Research
General rights

Infinity Sensor: Temperature Sensing in GaN Power Devices using Peak di/dt

Jianjing Wang, Mohammad H. Hedayati, Dawei Liu, Salah-Eddine Adami, Harry C. P. Dymond,
Jeremy J. O. Dalton, and Bernard H. Stark

Electrical Energy Management Group, Faculty of Engineering, University of Bristol, Bristol, United Kingdom
Bernard.Stark@bristol.ac.uk

Abstract — *Di/dt* has previously been proposed as a temperature indicator for Si and SiC devices, however, the evaluation of its viability for GaN devices is challenging as known current sensors introduce significant unwanted parasitic inductance. This work presents a figure-of-eight magnetic field sensor (∞ -sensor) that permits, for the first time, high-bandwidth floating current sensing, with negligible insertion impedance and influence on switching performance, in high-speed GaN and SiC switching circuits. The pair of coils are connected in a way that the measurement is immune to currents outside of the sensing region. The simulated bandwidth of the sensor, taking into account the loading by the probe connected to its output, is 225 MHz. The insertion inductance is 0.2 nH, and the insertion resistance is 4.2 mΩ at 100 MHz. This sensor is used to investigate the temperature dependency of turn-on *di/dt* in a 650 V, 52 mΩ GaN device. It is found that both average and peak turn-on *di/dt* decrease with temperature. Peak *di/dt* appears to be the preferred temperature indicator due to its high sensitivity and linearity.

Keywords — *Current sensing, Gallium nitride (GaN), Silicon carbide (SiC), Low insertion impedance, High bandwidth, Di/dt, Temperature.*

I. INTRODUCTION

Di/dt has been proposed as a temperature sensitive electrical parameter (TSEP) for silicon (Si) and silicon carbide (SiC) power devices [1]-[2]. For gallium nitride (GaN) devices, however, this potential temperature indicator has so far either not been investigated [3]-[5], or been considered unsuitable for temperature monitoring [6]. One of the barriers is the challenge of current sensing in GaN: First, high bandwidth is required as current transients exceed 10 A/ns [7]. Second, GaN switching waveforms are highly sensitive to parasitics, and therefore the insertion inductance

of the current sensor must be extremely low (sub-nH) so as to preserve typical switching waveforms [8]-[9]. Third, due to the extreme rates of change of current and voltage, noise immunity is a significant concern [10].

Various methods for measuring the current of wide bandgap (WBG) devices are compared in Table I. The current probe and current transformer used for Si and SiC measurement are too bulky for GaN in-circuit measurement, introducing excessive parasitic inductance [11]-[12]. The coaxial shunt from T&M Research so far has the highest bandwidth [13], however, it does not provide galvanic isolation and its insertion inductance of around 2 nH is large enough to significantly influence switching, for example [14] estimates a 67% increase in the power loop inductance of its 300-V GaN converter due to the use of this current shunt. Ten 0201 1-Ω resistors are paralleled to make a small current shunt in [15], however the measurement range is limited by its thermal dissipation [16], and the measurement accuracy is influenced by the frequency- and temperature-dependent resistance. Planar Rogowski coils in [17] and [18] allow galvanic isolation and continuous operation, and bandwidths of 170 MHz have been demonstrated. However, as they are embedded in the circuit board rather than standing alone as a discrete component, significant modifications to the circuit layout must be made, for example to the ground plane which leads to increased loop inductance.

This paper proposes a 225 MHz floating current sensor that requires only minor changes to the circuit layout in GaN converters. Its figure-of-eight shape and high-bandwidth lend it its name "∞-sensor", and it is based on a compensation concept described in [19] and [20], which is similar to how Rogowski coils work. Uniquely though, the ∞-sensor has been shown to provide accurate measurements without any

TABLE II. STATE-OF-THE-ART CURRENT MEASUREMENT METHODS.

Current sensing device	Bandwidth	Insertion resistance in Ω or V	Insertion inductance	Power device	Galvanic isolation	Sensing in control circuit
Split core current probe TCP0030A [11]	≥120 MHz	0.85 Ω at 120 MHz	> 10 nH	SiC	Yes	No
Current transformer Pearson 2877 [12]	200 MHz	0.02 Ω	N/A	SiC	Yes	No
Coaxial shunt SDN-414-10 [13]	2 GHz	0.1 Ω	2 nH	GaN/SiC	No	No
Virginia Tech SMD shunt [15]	N/A	0.1 Ω	N/A	GaN	No	Yes
Cambridge SMD shunt [16]	100 MHz	100 mV at full current	0.3 nH	GaN	No	Yes
Planar Rogowski coil [17]	100 MHz	N/A	N/A	SiC	Yes	Yes
Current sensor based on magnetic coupling [18]	170 MHz	N/A	N/A	GaN	Yes	Yes
∞-sensor (this work)	225 MHz	0.0042 Ω	0.2 nH	GaN/SiC	Yes	Yes

modification to the ground plane to the first inner PCB layer which carries the return current of a GaN power loop. As a result, insertion inductances of 0.2 nH or lower are possible, leading to current measurement being almost non-invasive. In this paper, the ∞-sensor's bandwidth and noise immunity are investigated, and the sensor is applied to a temperature-controlled bridge-leg converter consisting of 650 V, 52 mΩ GaN devices, in order to explore the sensor's viability for temperature sensing in GaN devices.

This paper is organised as follows: Section II presents the design of the ∞-sensor, including the concept, dimensions, and usage. Section III analyses and tests the performance of the sensor. Section IV demonstrates this sensor in a 400-V GaN converter, and investigates the temperature dependency of di/dt of the GaN device. Section V draws conclusions.

II. DESIGN OF THE ∞-SENSOR

A. Current sensing concept

The proposed ∞-sensor is illustrated in Fig. 1. The design concept is similar to a planar subset of a Rogowski coil, where the remaining coils have been moved laterally towards the conductor. A length of conductor carrying the current i_m to be measured is shown. The sensor consists of one planar coil on each side of the conductor, and sits right above the conductor to be measured. When the current flowing through the conductor changes, the consequent change in the magnetic field induces a voltage in the two planar coils. These two coils are connected in series so that the current in the trace directly under the middle of the sensor generates two signal components of the same polarity, thus providing a voltage signal v_{out} that is proportional to the change rate of the current, di/dt. v_{out} can be expressed as:

$$v_{out} = M \frac{di_m}{dt} \qquad (1)$$

where the sensor gain M is the mutual inductance between the ∞-sensor and the current loop which the current-carrying conductor is part of, and depends on the area of the coils and the relative position of the sensor coils and the conductor. The current to be measured i_m can thereby be derived as:

$$i_m = I_0 + \int \frac{v_{out}}{M} dt \qquad (2)$$

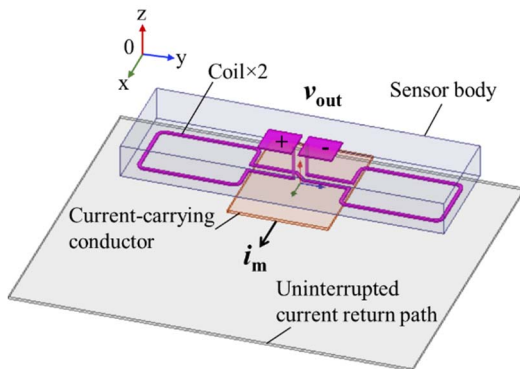where I_0 is the intial value of the current.

Fig. 1. Design concept of the ∞-sensor.

B. Dimensions

Both measurement gain and insertion impedance increase with the size of the coils. The sensor should be made only large enough to provide sufficient measurement gain, whilst being kept as small as practically possible to minimise insertion impedance. For fast-switching WBG devices with high di/dt, a balanced design can be found, as even small designs provide a reliably measurable output amplitude. For example, assuming that the current to be measured has a maximum rate of change of 10 A/ns, the sensor would generate an output voltage of around 1 V, if the sensor gain M is of the order of 0.1 V per A/ns.

The ∞-sensor adopted here and shown in Fig. 2 uses two symmetrical 1.5 mm × 2 mm coils and a 3-mm gap in between the coils. It is dimensioned specifically for GaN fast-switching devices. The coils are insulated using transparent high-temperature epoxy, onto which surface-mount pads are deposited for ease of assembly. The sensor is placed over a short piece of PCB trace between two components in order to measure the current in this section of trace. These sensor dimensions are suited to a track width of 3-6mm. The work presented in this paper uses a 70 μm thick, 3 mm wide and 4 mm long copper trace, which carries up to 20 A of current.
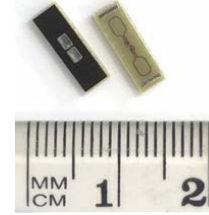

Fig. 2. Top and bottom view of an ∞-sensor.

C. Application in a GaN power converter

To use the ∞-sensor for measuring transient drain or source current of GaN devices in a bridge-leg converter, the current return plane (typically a ground plane on the first inner layer of a PCB) can be left intact as shown in Fig. 1, however components at either end of the trace to be measured need to be spaced out by 3.5 mm to permit the insertion of the sensor. The sensor is placed perpendicular to this trace, with the coils downwards and overlapping the trace on each side. The vertical distance of the coils to the trace is typically the thickness of the solder resist on the PCB, plus the epoxy insulation of the sensor (40 μm). No other current traces should be placed inside the footprint of the sensor. The output pads of the sensor on the top side can be connected to the oscilloscope either using a U.FL connector [21] and a coaxial cable or a twisted pair of wires through a probe. The measured current i_m can be calculated from the measured signal v_{out} using eqn. (2). In practice, the difference in the steady-state values of the current ΔI before and after the transient are typically known (e.g. the load current), which can be used to calibrate the sensor in situ. The sensor gain M is then ΔI divided by the sensor output signal integrated over the time period of the transient,

$$M = \frac{\Delta I}{\int v_{out} \, dt} \, . \qquad (3)$$
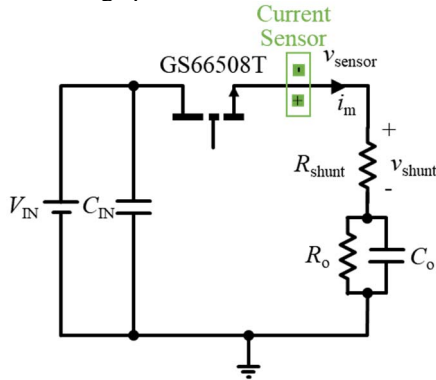
III. CHARACTERISATION OF THE ∞-SENSOR

A. ∞-sensor versus a shunt resistor

The simple GaN switching circuit of Fig. 3(a) is used to create a high-speed current pulse i_m to evaluate the ∞-sensor. The sensor is connected in series with a 1 Ω current shunt resistor for direct comparison. The width of the current carrying trace is 3 mm, as labelled in Fig. 3(b).

The ∞-sensor is first placed above the trace with the trace symmetrically aligned between the two coils. The output of

the sensor is connected directly through a U.FL connector and a 50 Ω coaxial cable to a Rhode & Schwarz RTO1024 2-GHz 10-GSa/s oscilloscope. The input impedance of this oscilloscope channel is selected to be 50 Ω to prevent ringing from impedance mismatch and wave reflections. This provides a 1:1 measurement with a relatively high signal-to-noise ratio. The voltage v_{shunt} across the shunt resistor is measured directly via a 500 MHz Rhode & Schwarz RT-ZP10 passive voltage probe.

(a) Schematic diagram.
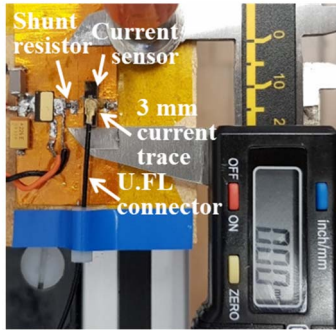
(b) Photo of the test board.

Fig. 3. A simple GaN test circuit for sensor characterisation.

The sensor output voltage v_{sensor}, the sensor current measurement i_{sensor} obtained by eqn. (2), and the shunt current measurement i_{shunt}, are shown in Fig. 4. It is apparent that the sensor measurement agrees well with that of the shunt resistor. The sensor gain M from eqn. (3) in this case is 105 mV per A/ns, and will be used as a baseline for the following evaluation. The test circuit achieves a peak di/dt of 5.6 A/ns, due to the limiting parasitic inductance of the series connected components of Fig. 3(a).
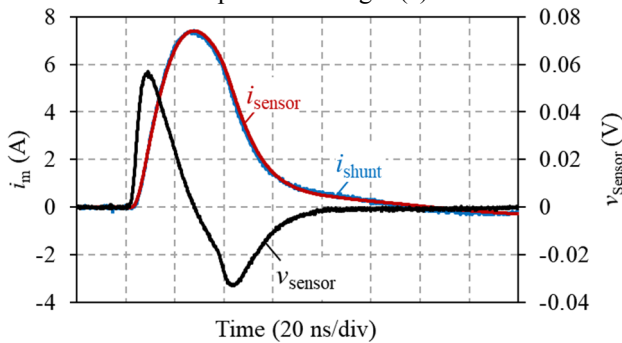

Fig. 4. Current measurement using series-connected shunt resistor and ∞-sensor.

B. Immunity to nearby currents

The immunity of the ∞-sensor to the currents in the vicinity is high for two reasons: First, currents with lower di/dt than that of the WBG devices result in proportionally lower sensor output voltage, according to eqn. (1). The WBG

devices usually have a peak di/dt of at least an order of magnitude higher than that of other currents on the circuit board. With its two turns and small surface area, the ∞-sensor has an innate immunity to adjacent currents with low rates of change. Second, the signals induced in each of the two series-connected turns partially cancel for current traces that lie outside of the sensor footprint, thus providing negligible total coupling, i.e., sensor gain M. The sensor's immunity to nearby currents can be analysed as follows:

Any currents flowing through traces, vias and pads on the circuit board can be decomposed into three components in the x-, y-, and z-directions respectively. First, as illustrated in Fig. 5, currents in the z-direction generate a magnetic field that is parallel to the sensor coils, resulting in zero coupling and thus no measurement output. Second, currents in the y-direction lying outside of the sensor footprint induce signals of opposite polarity in the two coils that cancel each other out, thus providing virtually no sensor output.
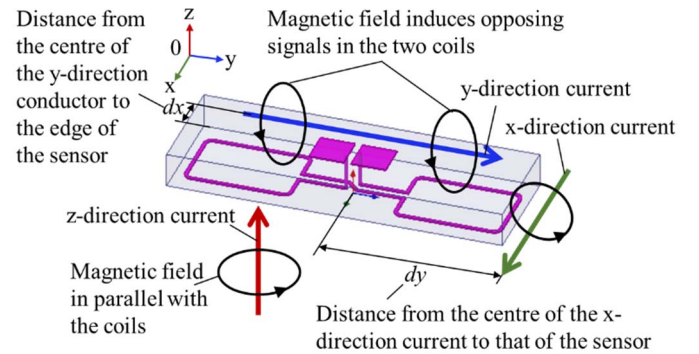

Fig. 5. Magnetic coupling between the sensor and the currents in the x-, y-, and z-directions.

The sensor's immunity to currents in the y-direction is measured and plotted in Fig. 6. The distance dx is that between the centre of the current trace and the closer edge of the sensor as illustrated in Fig. 5. This distance is swept from 0 to 8 mm. The measured sensor gain is shown to lie below 8.6 mV per A/ns. Noting that this equates to 8.2% of the 105 mV per A/ns output signal obtained from the correctly positioned measurement trace, and that it decreases with distance. This constitutes an acceptable immunity for many applications. For example, a current in y-direction that is 5 mm from the sensor provides an output that is less than 2% of the amplitude of a correctly aligned current in the x-direction.
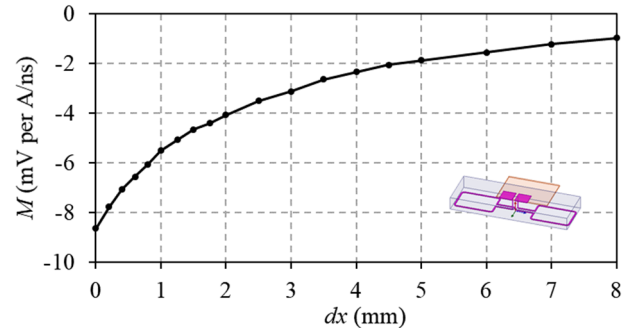

Fig. 6. Sensor gain M for a current in the y-direction against the distance dx of the current trace to the closer edge of the sensor.

Finally, the sensitivity to currents in the x-direction depends on the distance from the centre of the sensor, dy. This sensitivity is measured in a similar manner by sweeping the y-position dy of the sensor from 0 to 8 mm, and plotted in Fig. 7. Position $dy = 0$ corresponds to the perfectly aligned position of Fig. 5, also seen in Fig. 3(b). From $dy = 6.5$ mm

onwards, the current lies outside of the sensor footprint and the coupling M is virtually zero (below 6.19 mV per A/ns).
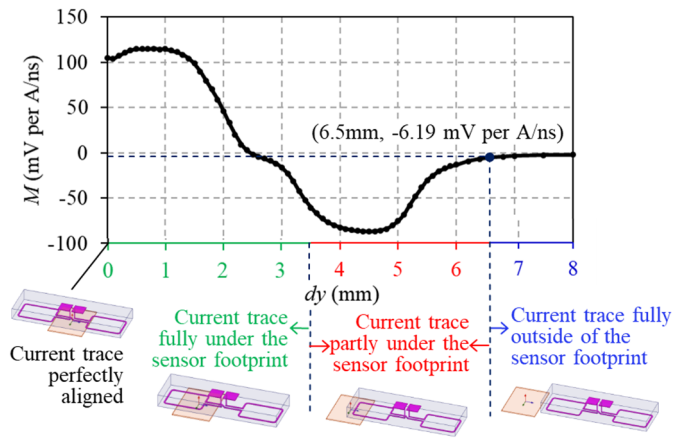

Fig. 7. Sensor gain M for a current in x-direction against y-position dy of sensor.

C. Sensitivity to position

In Fig. 7, the sensor gain M is seen to be approximately constant for the first 1.2 mm at either side of the perfectly aligned position, indicating that the sensor is relatively immune to small misalignments due to component placement tolerances. In this range, M varies by only 8.3%, and the sensor is insensitive to x-direction misalignment as long as the current distribution in this direction is even. A z-direction offset would reduce the measurement coefficient significantly. On the one hand, this may require sensor calibration on the board, as described in the previous section. On the other hand, it makes the sensor increasingly immune to currents on lower layers of the same board.

D. Insertion impedance, bandwidth, and galvanic isolation

To evaluate its performance in a practical fast-switching GaN circuit, the ∞-sensor is used to measure the drain current of the high-side 650 V GaN device in a bridge-leg converter as shown in Fig. 8(a). Each GaN device GS66508P is driven by a custom active gate driver [22] for fast switching speed with minimum oscillation.

Fig. 9 shows the PCB layout of the power conducting loop of the GaN bridge-leg test board in Fig. 8(b). As indicated by the white arrows, a 3 mm × 4 mm current-carrying trace is created on the top layer to accommodate the sensor. The first inner layer shown in green is an uninterrupted plane in which the current returns to the negative rail of the input capacitors. The distance between the trace and this plane is 127 μm.

The simulated parasitic power loop inductance and resistance at 100 MHz, with and without the current-carrying trace and the ∞-sensor, are compared in Table II. The additional trace is seen to increase the loop inductance by 0.2 nH and the loop resistance by 4.2 mΩ at frequencies of interest. These increases lie within 10% of the values without the additional trace.

The output of the sensor is connected to the Rhode & Schwarz RTO1024 2-GHz 10-GSa/s oscilloscope through a 500 MHz Rhode & Schwarz RT-ZP10 passive voltage probe. The bandwidth of the sensor is simulated in ADS (Agilent 2012) to be 225 MHz, taking into account the loading by the probe. The output inductor current is measured by a 100 MHz Keysight N2783B current probe, in order to provide the ΔI to calibrate the sensor according to eqn. (3).
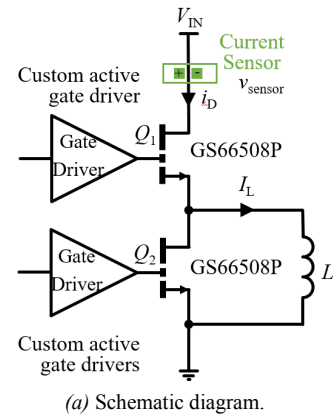
(a) Schematic diagram.
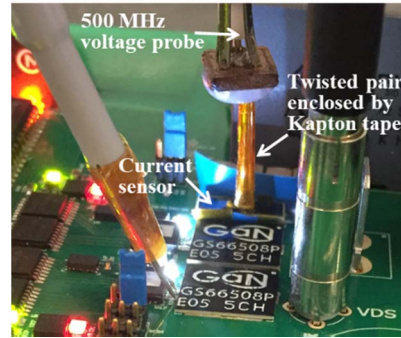
(b) Photo of the test board.

Fig. 8. A 400 V GaN bridge-leg circuit using the ∞-sensor at the high side.
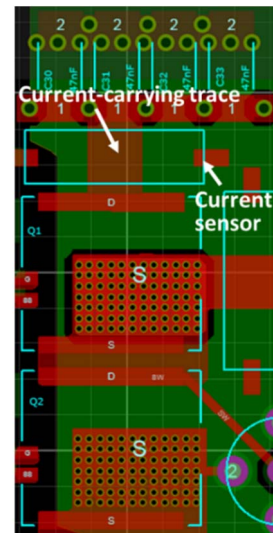

Fig. 9. PCB layout of power conducting loop. Red: top layer; green: the first inner layer.

TABLE II.   SIMULATED POWER LOOP IMPEDANCE AT 100 MHZ WITH AND WITHOUT THE CURRENT-CARRYING TRACE AND THE ∞-SENSOR.

Layout	Power-loop parasitic inductance	Power-loop parasitic resistance
with ∞-sensor	2.6 nH	42.0 mΩ
without ∞-sensor	2.4 nH	37.8 mΩ

Fig. 10 shows the measured sensor output voltage v_{Sensor} and drain current i_D at both turn-on and turn-off transients. The drain current is obtained according to eqn. (2), where the measurement coefficient is 125 mV per A/ns. It is different from the one in *Sec. III. A*, as the current-carrying traces and loops in these two test circuits differ. It is also demonstrated

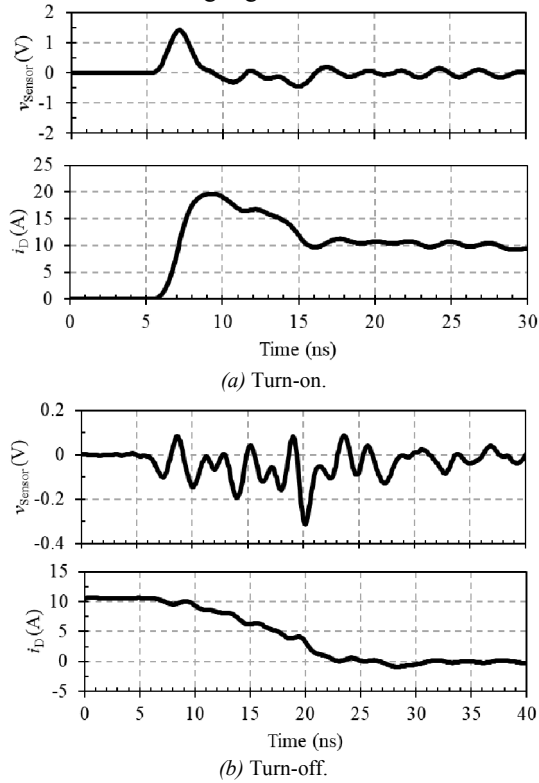that the ∞-sensor can provide galvanic isolation and measure the current at the floating high side.

(a) Turn-on.

(b) Turn-off.

Fig. 10. Measured sensor output voltage and high-side GaN FET transient drain current at both turn-on and turn-off.
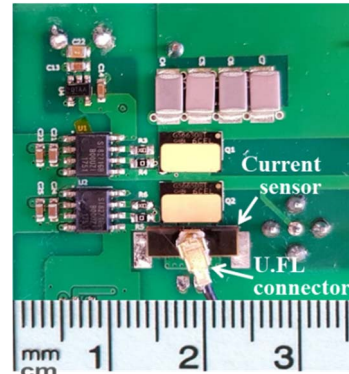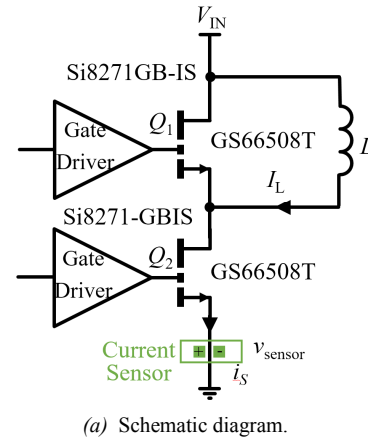
IV. TEMPERATURE DEPENDENCY OF GaN TURN-ON DI/DT

The 400 V GaN bridge-leg test circuit in Fig. 11 is used to investigate the temperature dependency of GaN turn-on di/dt, where the ∞-sensor measures the source current i_s of the low-side device. Each of the top-cooled GaN devices GS66508T is driven by an isolated gate driver Si8271GB-IS. The temperature of the GaN devices is set using a heater attached directly to the thermal pad of the GaN devices. The heater is controlled using an Inkbird ITC-100RL PID controller, with input from a thermocouple at the interface of the heater and the power devices. The temperature of the devices is additionally monitored by a FLIR E30 thermal camera. A double pulse test is taken at each temperature point after the device reaches thermal equilibrium. The output of the current sensor is connected through a U.FL connector and a 50 Ω coaxial cable to the oscilloscope. The output inductor current is measured by the Keysight N2783B current probe to provide the load current required for sensor calibration.

Fig. 12 shows the measured current sensor output voltage v_{sensor} and the inferred turn-on source current i_s, at 10 A output current, for device case temperatures ranging from 30°C to 150°C. The source current is inferred by eqn. (2), using a sensor gain of 105 mV per A/ns. The peak sensor output voltage and the rate of change of the current are lower than that in Fig. 10(a) at room temperature, and the current has greater current overshoot and oscillation.

It should be noted that this is because Fig. 10 uses active gate driving to shape the switching transient to obtain a fast switching speed with little current oscillation [22], whereas the work in this section uses non-active driving where switching speeds are slower and oscillation typically greater. The rate of change of the current is seen to decrease with the device temperature. Notably, the peak sensor output voltage

that corresponds to the peak di/dt also decreases with the device temperature.

(a) Schematic diagram.

(b) Bottom view of the test board with the GaN devices and the ∞-sensor.
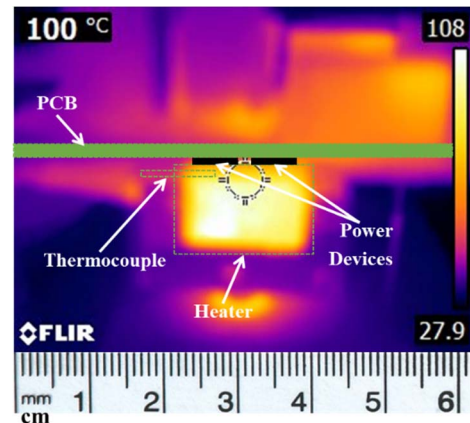
(c) Side view of the test setup for varying the GaN devices temperature.

Fig. 11. 400 V GaN test circuit for evaluating the temperature dependency of turn-on di/dt.
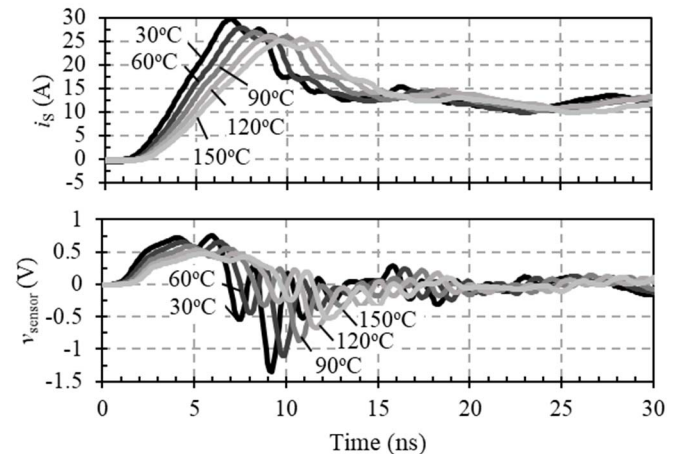

Fig. 12. Turn-on source current and the corresponding sensor output voltage against device temperature at 10 A output current.

Fig. 13 shows measured average di/dt between 10% and 90% rated current against the device temperature at different output currents. This parameter or its time equivalent of current rise time has been proposed as a temperature indicator for Si and SiC devices [1]-[2]. For the GaN device used here, the linear dependency on temperature at lower temperatures and lower currents decreases is seen to disappear.
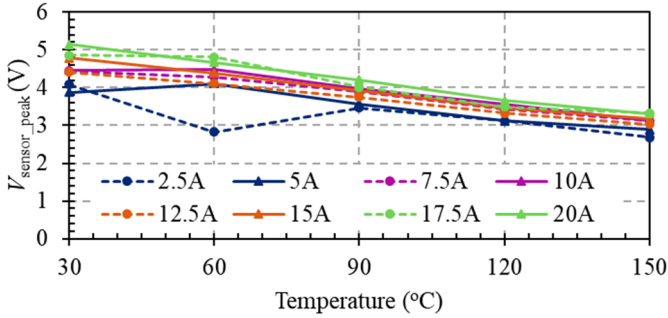

Fig. 13. Average di/dt against temperature at different output currents.

Fig. 14 shows the peak sensor output voltage v_{sensor_peak}, corresponding to peak di/dt, for the same measurements of Fig. 13. In contrast to Fig. 13, however, the peak di/dt shows a roughly linear dependency on temperature across the entire current and temperature range. As illustrated in Fig. 15, its temperature sensitivity shows little variation with the load current. Peak di/dt is therefore an interesting candidate for junction temperature sensing in GaN FETs. The ∞-sensor enables the reliable detection of this temperature indicator (TSEP) by using a peak-detect circuit.
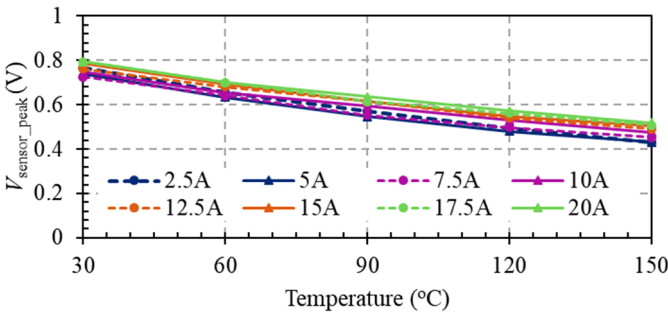

Fig. 14. Peak sensor output voltage against temperature at different output currents.
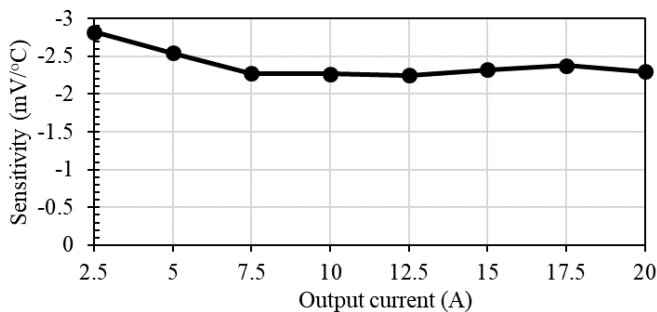

Fig. 15. Temperature sensitivity of peak sensor output voltage against converter output current.

A potential limitation of this method may be if the circuit displays significant current oscillation, in which case a peak di/dt during the current rise may be overshadowed by second non-temperature-dependent peak due to circuit resonance. The v_{sensor} waveform at 30°C in Fig. 12 shows the onset of this situation. This second peak could be mitigated without reducing the switching speed by waveform shaping via an active gate driver. In contrast, the waveforms of Fig. 10 show only one peak, and have been obtained with an active driver that cancels out current oscillation. Another

potential limitation of using di/dt as a temperature indicator is that it is a function of the gate threshold voltage, which in some GaN FETs has been reported to change with time when the gate is subjected to voltage stresses [23].

V. CONCLUSIONS

A figure-of-eight magnetic field sensor (∞-sensor) for measuring the transient current of WBG devices is presented in this paper. It fulfils the requirements on transient current sensing techniques for wide-bandgap power devices: compact size, high bandwidth, low insertion impedance, intrinsic noise immunity and galvanic isolation. The design concept is validated by a side-by-side comparison with a current shunt, an immunity and a sensitivity study, and by a demonstration of floating measurement in a practical 400 V GaN bridge-leg converter. Here, the ∞-sensor achieves a 225 MHz bandwidth and incurs only a 0.2 nH increase in the power loop inductance, as a result of adding a 3 mm gap for the sensor, either between DC-link capacitors and the high-side GaN FET, or the low-side GaN FET and the vias down to the current-return plane. In either case, the current-return (ground) plane remains uninterrupted, and is the first inner layer, with a 127 μm dielectric between this plane and the trace that carries the current being measured. The sensor is then used to investigate the temperature dependency of turn-on di/dt in a GaN bridge-leg converter. It is demonstrated that both average and peak di/dt decrease with increasing device temperature. The ∞-sensor concept could also be embedded into the circuit board if appropriate. The 10×3 mm ∞-sensor used in this paper could be used for wider tracks up to 6 mm, or miniaturised to further reduce the insertion impedance.

REFERENCES

[1] J. O. Gonzalez, O. Alatise, J. Hu, L. Ran, and P. A. Mawby, "An Investigation of Temperature-Sensitive Electrical Parameters for SiC Power MOSFETs," *IEEE Trans. Power Electron.*, vol. 32, No. 10, pp. 7954–7966, Oct. 2017.

[2] A. Griffo, J. Wang, K. Colombage, and T. Kamel, "Real-Time Measurement of Temperature Sensitive Electrical Parameters in SiC Power MOSFETs," *IEEE Trans. Ind. Electron.*, vol. 65, No. 3, pp. 2663–2671, Mar. 2018.

[3] L. Zhang, P. Liu, S. Guo, and A. Q. Huang, "Comparative study of temperature sensitive electrical parameters (TSEP) of Si, SiC and GaN power devices," in *IEEE Workshop on Wide Bandgap Power Devices and Applications (WiPDA)*, Nov. 2016, pp. 302–307.

[4] S. Wang, F. Xue, A. Q. Huang, and S. Liu, "Physics understanding of high temperature behavior of gallium nitride power transistor," in *IEEE Workshop on Wide Bandgap Power Devices and Applications (WiPDA)*, Nov. 2016, pp. 324–327.

[5] J. Franke, G. Zeng, T. Winkler, and J. Lutz, "Power cycling reliability results of GaN HEMT devices," in *IEEE International Symposium on Power Semiconductor Devices IC's (ISPSD)*, May 2018, pp. 467-470.

[6] S. Zhu, A. Fayyaz, and A. Castellazzi, "Static and dynamic TSEPs of SiC and GaN Transistors," in *International Conference on Power Electronics, Machines and Drives (PEMD)*, Apr. 2018, pp. 1–6.

[7] E. A. Jones, "Review and characterization of gallium nitride power devices," Master's Thesis, University of Tennessee, 2016.

[8] D. Reusch and J. Strydom, "Understanding the effect of PCB layout on circuit performance in a high-frequency gallium-nitride-based point of load converter," *IEEE Trans. Power Electron.*, vol. 29, No. 4, pp. 2008–2015, Apr. 2014.

[9] J. Lautner and B. Piepenbreier, "Impact of current measurement on switching characterization of GaN transistors," in *Proc. IEEE WiPDA*, 2014, pp. 98–102.

[10] S. Ziegler, R. C. Woodward, H. H.-C. Iu, and L. J. Borle, "Current sensing techniques: A review," *IEEE Sensors J.*, vol. 9, no. 4, pp. 354–376, Apr. 2009.

[11] Tektronix Inc. TCP0030A Datasheet. [Online]. Available: http://www.tek.com/

[12] Pearson Electronics application note, "Effect of Current Monitors on Circuit Inductance," Apr. 1996.

[13] T&M Research Products, Inc. *SSDN-414-10*. [Online]. Available: http://www.tandmresearch.com/

[14] B. Sun, R. Burgos, X. Zhang, and D. Boroyevich, "Active dv/dt control of 600V GaN transistor," in *Proc. IEEE Energy Conversion Congress Exposition (ECCE)*, Sep. 2016.

[15] M. Danilovic, Z. Chen, R. Wang, F. Luo, D. Boroyevich, and P. Mattavelli, "Evaluation of the switching characterstics of a gallium-nitride transistor," in *Proc. IEEE Energy Conversion Congress Exposition (ECCE)*, Sep. 2011, pp. 2681–2688.

[16] E. Shelton, X. Zhang, T. Zhang, N. Hari, and P. Palmer, "Low inductance switching for SiC MOSFET based power circuit," in *Proc. IEEE Energy Conversion Congress Exposition (ECCE)*, Oct. 2017, pp. 2681–2688.

[17] Y. Xue, J. Lu, Z. Wang, L. M. Tolbert, B. J. Blalock, and F. Wang, "A compact planar Rogowski coil current sensor for active current balancing of parallel-connected silicon carbide MOSFETs," in *Proc. IEEE Energy Conversion Congress Exposition (ECCE)*, Sep. 2014, pp. 4685–4690.

[18] K. Wang, X. Yang, H. Li, H. Ma, X. Zeng, and W. Chen., "An analytical switching process model of low-voltage eGaN HEMTs for loss calculation," *IEEE Trans. Power Electron.*, vol. 31, no. 1, pp. 635–647, Jan. 2016.

[19] P. R. Palmer, B. H. Stark, and J. C. Joyce, "Non-invasive measurement of chip currents in IGBT modules," in *Proc. Power Electronics Specialists Conf.*, 1997, pp. 166–171.

[20] F. G. M. De Jong., "Method of testing a connection which includes a conductor in an integrated circuit," WO1997046891A1, Dec. 11, 1997.

[21] Hirose U.FL. https://en.wikipedia.org/wiki/Hirose_U.FL

[22] J. Wang, D. Liu, H. C. P. Dymond, J. J. O. Dalton, and B. H. Stark, "Crosstalk suppression in a 650-V GaN FET bridgeleg converter using 6.7-GHz active gate driver," in *Proc. IEEE Energy Conversion Congress Exposition (ECCE)*, Oct. 2017, pp. 1955–1960.

[23] J. Lutz, H. Schlangenotto, U. Scheuermann, and R. De Doncker, *Semiconductor Power Devices: Physics, Characteristics, Reliability*, 2nd edition, Springer, 2018.